JACS
JOURNAL OF THE AMERICAN CHEMICAL SOCIETY

Article

pubs.acs.org/JACS

Autonomic Molecular Transport by Polymer Films Containing Programmed Chemical Potential Gradients

Chunjie Zhang,[†,∥,◆] Amit Sitt,[‡,◆] Hyung-Jun Koo,[†,⊥] Kristopher V. Waynant,[†,#] Henry Hess,[*,‡] Brian D. Pate,[§] and Paul V. Braun[*,†]

[†]Department of Materials Science and Engineering, Beckman Institute for Advanced Science and Technology, Frederick Seitz Materials Research Laboratory, University of Illinois at Urbana—Champaign, Urbana, Illinois 61801, United States

[‡]Department of Biomedical Engineering, Columbia University, 1210 Amsterdam Avenue, New York, New York 10027, United States

[⊥]Department of Chemical & Biomolecular Engineering, Seoul National University of Science and Technology, 232 Gongneung-ro, Nowon-gu, Seoul 139-743, Korea

[§]Defense Threat Reduction Agency, Fort Belvoir, Virginia 22060, United States

Supporting Information

ABSTRACT: Materials which induce molecular motion without external input offer unique opportunities for spatial manipulation of molecules. Here, we present the use of polyacrylamide hydrogel films containing built-in chemical gradients (enthalpic gradients) to direct molecular transport. Using a cationic tertiary amine gradient, anionic molecules were directionally transported up to several millimeters. A 40-fold concentration of anionic molecules dosed in aerosol form on a substrate to a small region at the center of a radially symmetric cationic gradient was observed. The separation of mixtures of charged dye molecules was demonstrated using a boronic acid-to-cationic gradient where one molecule was attracted to the boronic acid end of the gradient, and the other to the cationic end of the gradient. Theoretical and computational analysis provides a quantitative description of such anisotropic molecular transport, and reveals that the gradient-imposed drift velocity is in the range of hundreds of nanometers per second, comparable to the transport velocities of biomolecular motors. This general concept of enthalpy gradient-directed molecular transport should enable the autonomous processing of a diversity of chemical species.

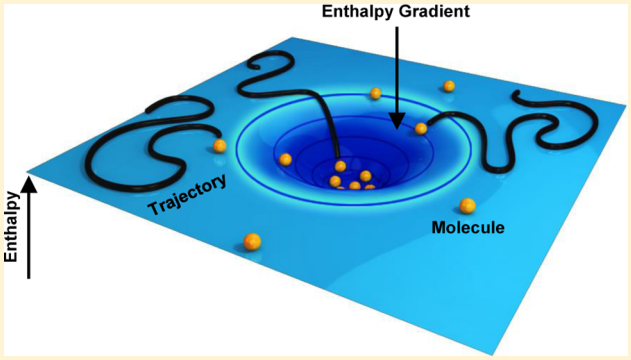

INTRODUCTION

Microscale manipulation of chemicals and biological species (e.g., cells) is now possible via lab-on-a-chip technologies. Such devices boast many attractive features, including precise operations on small quantities of materials, low energy consumption, and rapid process steps, which have made them valuable for chemical, biological and medical applications.[1−4] A key feature of lab-on-a-chip devices is the ability to transport the agent of interest, typically through moving fluids and externally applied electrical fields. New paradigms for directional molecular transport based on internal inputs, which provide a level of autonomy, such as molecular motors,[5−7] and surface patterned chemical gradients, rather than through externally applied inputs, are now emerging. The anisotropic motion of liquid droplets and cells on gradient surfaces was first reported a number of years ago.[8−14] However, the gradient-driven anisotropic transport of molecular-scale objects has been limited to transport on the surface of solids immersed in liquids. For example, nanoparticles,[15] a poly(propyleneimine) dendrimer,[16] poly(ethylene glycol),[17] and adamantine-appended dye molecules[18] have all been transported via such strategy. Here we demonstrate a gradient-directed molecular transport strategy in which molecules are transported within a hydrogel film containing embedded chemical gradients. This approach is particularly attractive for manipulating chemical species deposited out of the air, and more generally does not require the substrate to be immersed in a liquid. Here, millimeter scale lateral transport of molecules was directed through both charge and chemically specific interactions using hydrogel films which were prepatterned with embedded lateral chemical gradients. Along with being an important demonstration of chemically specific transport in hydrogels, this is also a powerful demonstration of gradient-directed concentration of molecules and gradient-directed separation of mixtures of molecules.

The concept of autonomic gradient-driven molecular transport inside swollen polymer films was in part inspired by gel electrophoresis, where the gel serves as the transport medium and the externally applied electric field provides the driving

Received: January 12, 2015
Published: March 16, 2015

DOI: 10.1021/jacs.5b00240
J. Am. Chem. Soc. 2015, 137, 5066−5073

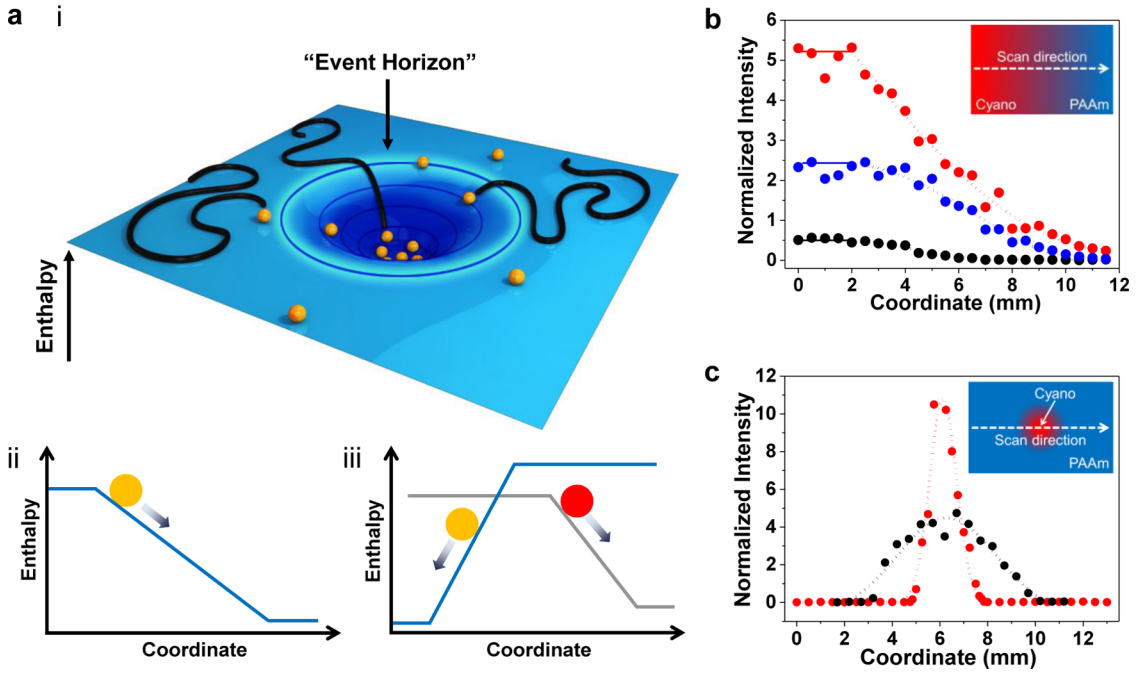

Figure 1. Function and characterization of chemical gradients. (a) i. Schematic illustration of the directed transport of molecules (depicted as orange spheres) by a two-dimensional radially symmetric enthalpy gradient. Molecules outside of the gradient exhibit only random diffusion. The curved blue surface represents the enthalpy profile of the molecule in the medium. Black lines are illustrated trajectories of selected molecules. ii. A molecule moves from a high enthalpy region to a low enthalpy region. iii, Directed separation of a binary mixture (formed by molecules represented by the orange and red sphere) by the enthalpy gradient of each component. (b) Normalized cyano peak intensity along directional cyano gradients fabricated using hydrolysis times of 24 h (red), 12 h (blue) and 2.5 h (black). (c) Normalized cyano peak intensity along narrow (red) and wide (black) radially symmetric cyano gradients. Raman spectra in (b) and (c) were normalized by the C—C stretch of PAAm backbone at ca. 1096 cm^{-1}.

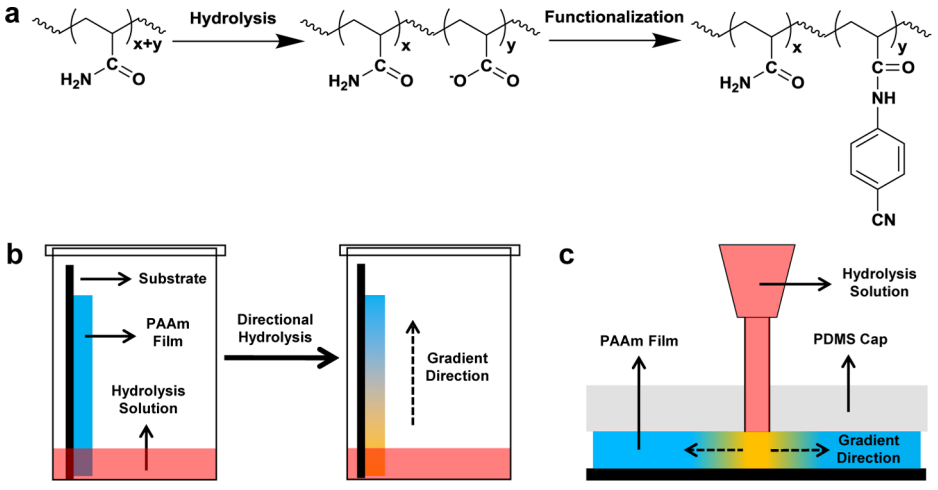

Figure 2. Chemical gradient fabrication in PAAm hydrogel films. (a) Synthetic route for cyano gradients as model systems for Raman Spectroscopic characterization. The *x* represents the molar percentage of pristine PAAm repeating units, and *y* represents the molar percentage of carboxylates in the hydrolyzed PAAm hydrogel and the molar percentage of the cyano functionality in the final gradient hydrogel, assuming the functionalization step has a high conversion yield. (b,c) Experimental setups for localized hydrolysis for creating directional and radially symmetric chemical gradients in PAAm hydrogel films.

force for molecular transport.[19,20] The rationale for embedding the chemical gradient inside a hydrogel, rather than using an externally applied field is 2-fold. First, the complex spatial control of analyte motion can be achieved (e.g., focusing of molecules to a region of the hydrogel), and second, and perhaps more significant, chemically specific, rather than generic electric field interactions can be used to drive molecular transport. Another important motivation for gradient-directed molecular transport was a prior report that showed nanoscale sensors have limited sensitivity if analyte transport is purely diffusive since the probability that a molecule will intersect with a nanosized sensor is very low when the concentration of molecules in the vicinity of the sensor is low.[21] Directed transport of analyte to nanoscale sensors would greatly improve both the sensitivity and response time by increasing the concentration of molecules near the sensor, and the probability that the analyte intersects with the sensor.[22,23]

DOI: 10.1021/jacs.5b00240
J. Am. Chem. Soc. 2015, 137, 5066−5073

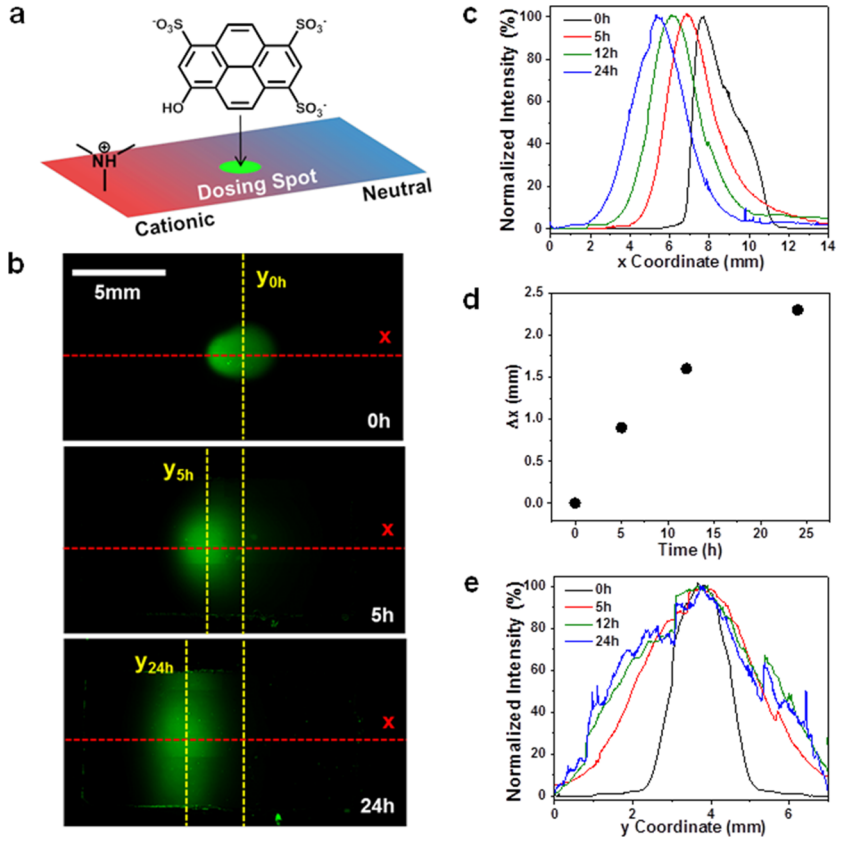

Figure 3. Directed molecular transport by a hydrogel film containing a directional enthalpy gradient. (a) Schematic illustration of a PAAm hydrogel film containing a directional cationic-to-neutral gradient dosed with pyranine. (b) Fluorescence images taken during the directed transport of pyranine by the cationic-to-neutral gradient over time. (c) Normalized fluorescence intensity profile along the gradient (*x*-coordinate). (d) The distance that the fluorescence intensity maximum moves along the *x*-coordinate (Δx) in (c) as a function of time. (e) Normalized fluorescence intensity profile perpendicular to the gradient (*y*-coordinate). The *y*-coordinates used to plot the fluorescence intensity at 5 and 24 h are indicated by the yellow dashed lines labeled as y_{5h} and y_{24h} in (b), respectively.

Directed molecular transport may also improve targeted drug delivery[24,25] and provide an approach to localize chemical reactions to specific locations. Importantly, the enthalpy gradient which results from the chemical gradient is chemically specific, and thus chemically distinct molecules can be transported in different directions under the same chemical gradient. The net molecular transport by an enthalpy gradient can be against the concentration gradient (Figure 1ai). Enthalpy gradients based on various interactions, including electrostatic, hydrogen bonding, and supramolecular forces can be interlaced in the same hydrogel, providing the opportunity to concurrently and selectively manipulate different analytes.

In this study, polyacrylamide (PAAm) hydrogels were selected as the molecular transport media due to their flexibility for chemical modification and relatively inert nature. For all experiments, ca. 30 μm thick hydrogel films were chemically coated on acrylate-functionalized glass substrates. The high water content of the hydrogel (over 90%) results in diffusion coefficients comparable with those in aqueous solutions.[26] To generate chemical gradients, amides in PAAm were first locally hydrolyzed, yielding a gradient of carboxylates (Figure 2a). The slow hydrolysis kinetics of PAAm at room temperature provides control over the hydrolysis degree at selected locations, enabling various gradient strengths, geometries, and scales. The carboxylates were then converted to desired functionalities through conjugation with amine-appended molecules, creating a variety of chemical gradients in PAAm hydrogel films (Figure 2a).

RESULTS AND DISCUSSION

Gradient Fabrication and Characterization. Directional and radially symmetric cyano gradients fabricated by conjugating 4-aminobenzonitrile to carboxylate gradients generated by localized hydrolysis of PAAm films were used as model systems for Raman microscopy (Figure 2a). The geometry of cyano gradients was controlled during the hydrolysis step by applying different localized hydrolysis approaches (Figure 2b,c).

The cyano group exhibits a distinct stretch peak at ca. 2228 cm^{-1},[27−29] enabling the quantification of its content at selected locations along the gradient. All Raman spectra were normalized by the C—C stretch of the PAAm backbone at ca. 1096 cm^{-1}.[30] Nearly linear gradients were formed with the slope controlled by the reaction conditions (Figure 1b, Supporting Information, SI, Figure S3a for the complete normalized Raman spectra). Spatial control over the hydrolysis reaction can be used to form different gradient geometries. For example, Figure 1c shows the C≡N stretch peak intensity across radially symmetric gradients (SI Figure S3b for the complete normalized Raman spectra). Note, all hydrogel films described in this paper are thin (ca. 30 μm) compared to their lateral dimensions (several millimeters), and thus, can be considered two-dimensional.

DOI: 10.1021/jacs.5b00240
J. Am. Chem. Soc. 2015, 137, 5066−5073

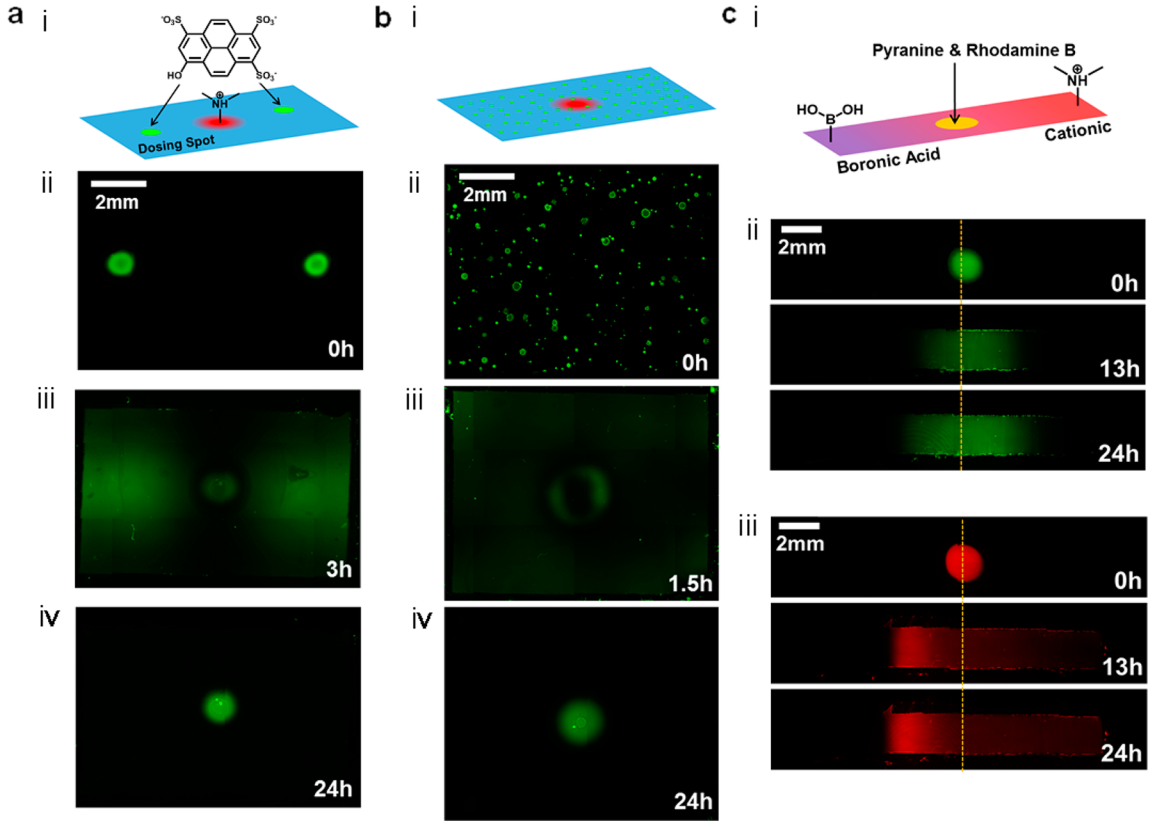

Figure 4. Directed molecular concentration and separation by hydrogel films with programmed enthalpy gradients. (a) i. Schematic illustration of a PAAm hydrogel film containing a radially symmetric cationic-to-neutral gradient dosed with two spots of pyranine. ii–iv, Fluorescence images during the directed concentration of pyranine by the radial cationic-to-neutral gradient. (b) i. Schematic illustration of a PAAm hydrogel film containing a radially symmetric cationic-to-neutral gradient dosed with discrete pyranine spots using atomizer spray. ii. Fluorescence image of the dry PAAm film sprayed with pyranine. iii–iv. Fluorescence images during the directed concentration of pyranine. (c) i. Schematic illustration of the dosing of a dye mixture on a directional boronic acid-to-cationic (left to right) gradient. Fluorescence images of ii pyranine and iii rhodamine B during the directed separation of the binary mixture by the PAAm hydrogel film containing boronic acid-to-cationic gradient.

Gradient-Directed Transport. Enthalpy gradients of electrostatic interactions were selected to drive the anisotropic movement of pyranine, an anionic fluorescent probe used for visualizing the transport at selected time points. The rectangular PAAm hydrogel film was cationic (functionalized with *N*,*N*-dimethylethylenediamine) on one end and neutral (pristine PAAm) on the other, with a cationic-to-neutral gradient in between. The gradient was fabricated by hydrolyzing a pristine PAAm film from one end and then conjugating with *N*,*N*-dimethylethylenediamine, similar to the preparation of directional cyano gradients as shown in Figure 2a,b. The hydrogel film was equilibrated in pH 7.4 phosphate buffered saline (PBS) and then dosed with pyranine (Figure 3a). Fluorescence images were taken as a function of time under 100% relative humidity (Figure 3b). The synthetic and experimental details are provided in SI Section 2.3. The pyranine spot spread both along and perpendicular to the gradient direction over time. The transport along the *x*-coordinate (gradient direction) is anisotropic (Figure 3c) due to the molecular movement to the low enthalpy region of the PAAm film, as illustrated in Figure 1aii. As can be seen in Figure 3d, the fluorescence intensity maximum moves ca. 0.9 mm along the *x*-coordinate within 5 h and ca. 2.3 mm within 24 h. The transport along the *y*-coordinate (perpendicular to the gradient) is isotropic, as indicated by the symmetric fluorescence profile at selected time spots (Figure 3e).

Gradient-Directed Concentration. A radial cationic-to-neutral gradient was prepared by radially symmetric localized hydrolysis of a PAAm film followed by conjugation with *N*,*N*-dimethylethylenediamine, similar to the preparation of radially symmetric cyano gradients as indicated in Figure 2a and 2c (SI Section 2.3 for synthetic details). Pyranine was dosed at two spots outside of the gradient (Figure 4, parts ai–ii). The fluorescence intensity of the two dosing spots initially decreased over time as pyranine isotropically diffused into the surrounding hydrogel medium. However, once pyranine crossed the "event horizon", which is the outer edge of the gradient, it was directed to the gradient center (Figure 1ai and Figure 4aiii). A depletion region can be clearly observed as a dark circle surrounding the gradient during the directed concentration, as shown in Figure 4aiii. This is an inherent feature of gradient-driven transport and occurs when molecules move from a region of concentration gradient-induced transport to a region of enthalpy gradient-induced transport. When molecules reach the depletion region, they are swept inward by the gradient faster than they are replaced by the free diffusion from the surroundings, leading to a dark ring at the outer edge of the gradient. After 24 h, the highest fluorescence intensity was observed at the cationic center of the gradient (Figure 4aiv). To mimic an aerosol dosing event, pyranine was sprayed on a dry PAAm film containing a radially symmetric cationic-to-neutral gradient pretreated with pH 7.4 PBS (Figure 4bi). Pyranine landed on the dry gradient film as immobilized

DOI: 10.1021/jacs.5b00240
J. Am. Chem. Soc. 2015, 137, 5066–5073

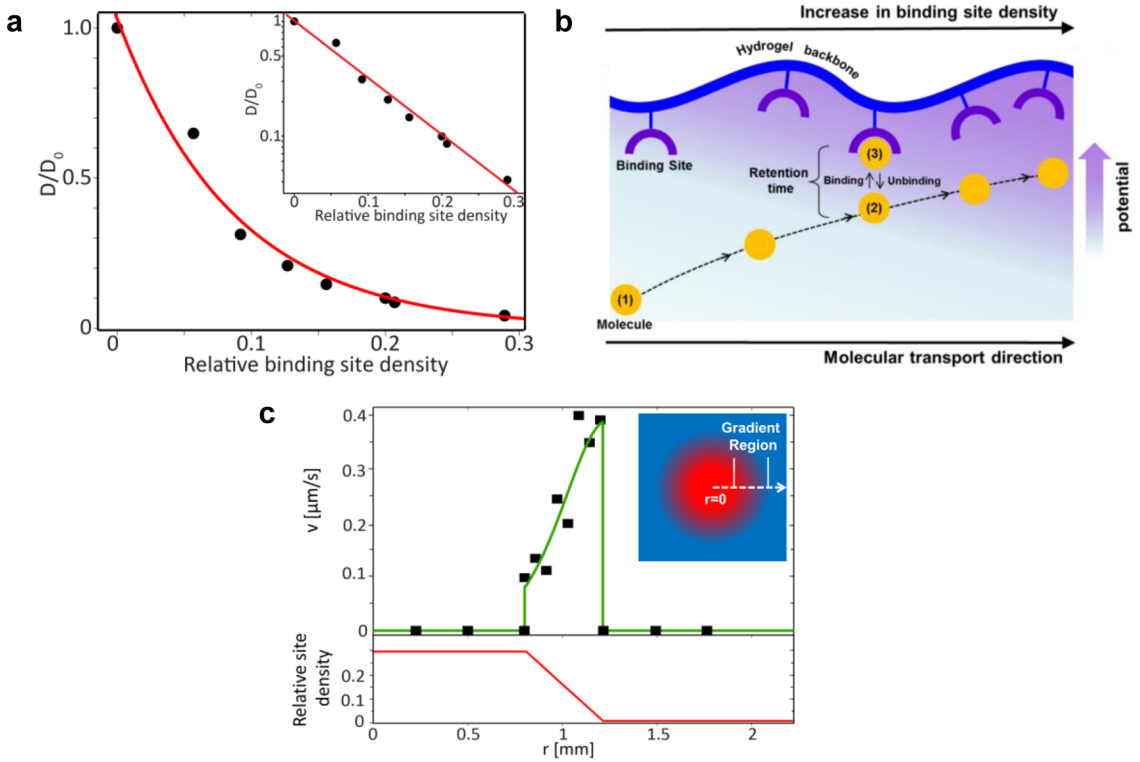

Figure 5. Fundamental parameters for enthalpy gradient-driven molecular transport. (a) Experimentally measured diffusion coefficient of pyranine as a function of binding site density obtained from pyranine diffusing in homogeneous cationic PAAm hydrogel films with varied binding site densities (black circles). The data fits to a single exponential (red solid line), as is demonstrated by the semilog representation (inset). (b) Schematic representation portraying the mechanism for gradient-induced transport in hydrogels. A molecule approaching the polymer backbone (1) can associate with a binding site (3), decreasing the mobility of the molecule. When unbound and mobile (2), the molecule moves along the gradient due to the electrostatic potential exerted on it by the ionic binding sites on the hydrogel backbone. (c) The radially symmetric velocity profile obtained through trajectory optimization (upper panel black squares) and from the suggested theoretical model (upper panel green solid line). Lower panel depicts the binding site density along the hydrogel patch shown schematically in the inset.

discrete spots (Figure 4bii). The dosed gradient-containing film was then transferred to a sealed chamber with 100% relative humidity to hydrate the hydrogel and initiate the directed concentration. The depletion region here was also clearly visible (Figure 4biii). After 24 h, pyranine was concentrated to the center, as indicated by the bright circular region on the fluorescence images (Figure 4biv). As expected, the hydrogel film with a narrow gradient (Figure 4, parts bii–iv) confined the dye to a smaller region compared to the film with a wide gradient (SI Figure S7a). The geometry of the radially symmetric gradient is defined in SI Figure S8. As a control, the same experiment was conducted on a pristine PAAm film and directed concentration was not observed (SI Figure S7b).

The directed concentration was quantified by Raman spectroscopy using 1,3,6,8-pyrenetetrasulfonate (PyTS) as the molecular probe on radially symmetric cationic-to-neutral gradients. PyTS has four sulfonate groups which are negatively charged at pH 7.4 (SI Figure S6). Using an atomizer, PyTS was sprayed on a dry PAAm film containing radially symmetric cationic-to-neutral gradient and a dry pristine PAAm film. During the directed concentration at 100% relative humidity, Raman spectroscopy was performed at selected time points (SI Figure S9a–c). The aromatic structure of PyTS provides distinct Raman signals (ca. 1217, 1331, and 1632 cm^{-1})[31,32] which after 21 h were clearly visible at the gradient center, while for PyTS dosed on the pristine PAAm film, the Raman signals were much lower (SI Figure S9i–k). The concentration enhancement ratio is defined as the intensity of the PyTS Raman signal at the center of the radially symmetric gradient divided by the average PyTS intensity on the pristine PAAm film. The concentration enhancement ratio by a gradient with diameter d of ca. 0.5 mm and length L of ca. 1.0 mm is 40 (SI Figure S9a–d), while the concentration enhancement by a wider radial gradient (d of ca. 0.5 mm, L of ca. 1.75 mm) is 14 (SI Figure S9e–h). Assuming the gradient center is a perfect sink, the upper bound of the concentration enhancement ratio can be estimated as the total area of the hydrogel film to the area of the cationic center (upper bound = $(4T/\pi d^2)$ = 315 for both gradients, T stands for the area of the entire hydrogel film). The experimentally observed values (40 for the narrow gradient and 14 for the wide gradient) are below the upper bound probably because the equilibrium has not been reached and the gradient center has limited capacity.

Gradient-Directed Separation. Different enthalpy profiles of molecules on a gradient make chemical separation possible, since each molecule follows its chemically specific downhill movement to low enthalpy regions (Figure 1aiii for a schematic representation). As a proof-of-concept, a binary mixture of 0.3 mM rhodamine B and 0.3 mM pyranine was separated by a PAAm hydrogel film functionalized with noninteracting (orthogonal) chemical gradients. While orthogonal gradients may not be necessary for all separations, they open up the possibility for arbitrary spatial control of separation. The excitation and emission wavelengths of rhodamine B and pyranine do not overlap, which allows following their transport using fluorescence imaging simultaneously during the directed

DOI: 10.1021/jacs.5b00240
J. Am. Chem. Soc. 2015, 137, 5066–5073

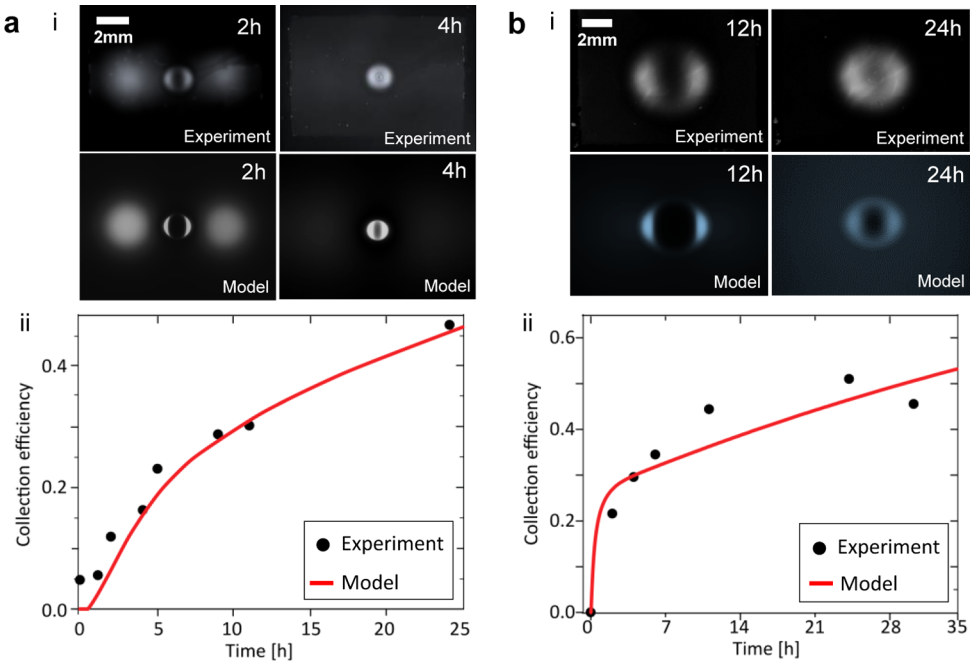

Figure 6. Experimental and modeled directed molecular concentration. (a) i, Experimental fluorescence images (upper panel) and modeled concentration maps (lower panel) of pyranine in a PAAm hydrogel film containing a narrow cationic-to-neutral (tertiary amine-to-pristine PAAm) gradient. ii, Experimental (circles) and modeled (solid line) collection efficiency of pyranine by the cationic (tertiary amine) gradient region as a function of time for the narrow gradient. (b) i, Experimental fluorescence images (upper panel) and modeled concentration maps (lower panel) of pyranine in a PAAm hydrogel film containing a wide cationic-to-neutral (tertiary amine-to-pristine PAAm) gradient. ii, Experimental (circles) and modeled (solid line) collection efficiency of pyranine by the cationic (tertiary amine) gradient region as a function of time for the wide gradient.

separation. 0.1 μL of the binary dye mixture was dosed as an ca. 2 mm diameter spot in the middle of a pH 7.4 PBS treated PAAm hydrogel film consisting of 3-aminomethylphenylboronic acid (3AmPBA) and *N*,*N*-dimethylethylenediamine end functionalities and a boronic acid-to-cationic gradient in between (Figure 4ci). The detailed fabrication and experimental procedures are provided in SI Section 2.4. 3AmPBA was selected over other boronic acids because of its hydrophilicity which maintains the hydrogel morphology and water content. On the boronic acid-to-cationic gradient, rhodamine B was directed to the 3AmPBA side of the gradient due to the interactions of its tertiary amines with the immobilized boronic acid,[33] while pyranine moved toward the cationic side driven by the electrostatic interactions (Figure 4, parts cii–iii). After 24 h, the molar ratio of rhodamine B to pyranine to the left of the dosing spot was ca. 3:1, as estimated from fluorescence images. Detailed discussions on the quantification of separation are provided in SI Section 2.4.

Theory and Modeling. To better understand the gradient-driven transport, a two-dimensional diffusion-convection equation was used to model the systems,

$$\frac{\partial c}{\partial t} = \nabla\cdot[D(x, y)\nabla c] + \nabla\cdot[\vec{v}(x, y)c] \quad (1)$$

where $D(x, y)$ is the local diffusion coefficient, $\vec{v}(x, y)$ is the gradient-imposed drift velocity, and c is the molecule's concentration. Both the diffusion coefficient and drift velocity change as a function of position, and are related to binding site density $\rho(x, y)$ in the gradient. Since the binding site density varies slowly with position, we assume the local diffusion coefficient is similar to that of the molecule in a homogeneous hydrogel with the same binding site density. To obtain D along the gradient, a series of measurements was performed in hydrogels with homogeneous binding site densities (SI Section 7). Figure 5a shows that D of pyranine in homogeneous cationic PAAm films is well-fitted by a single exponential function of the molar concentration of binding sites.

While the diffusion coefficient D is determined experimentally, establishing an expression for the drift velocity requires the construction of a theoretical framework (SI Section 8). Several works have presented models for diffusion in gels[26] considering the effects of obstruction, specific binding,[34] and electrostatic potential in charged systems.[35,36] For hydrogel systems in this study, the electrostatic sites are introduced after the polymer backbone is formed so the obstruction effect should be similar for all systems. Inside the gradient, cargo molecules can be either docked to a binding site on the polymer backbone, or in an unbound state in the pore (Figure 5b). The binding hinders diffusion, resulting in a decrease in the diffusion coefficient with respect to the pristine PAAm hydrogel. The electrostatic sites on the polymer backbone induce an electrostatic potential on the cargo molecules. Such electrostatic gradient in the hydrogel translates to a potential gradient, resulting in a force exerted on the cargo molecule toward high binding site density direction.

To obtain an explicit expression for the velocity, we assume that it is related to the force, $F(x_0, y_0)$, which is locally exerted by the potential gradient, through a local manifestation of the Einstein-Smolochowski relation, commonly used for homogeneous systems. Using this relation, the velocity is expressed as

$$v(x_0, y_0) = \frac{1}{k_B T} D(x_0, y_0) F(x_0, y_0) \quad (2)$$

To the first approximation, the energy is linearly proportional to the binding site density, $U(x_0, y_0) = Q\rho(x_0, y_0)$, with Q being the proportionality factor. Consequently, the force is propor-

DOI: 10.1021/jacs.5b00240
J. Am. Chem. Soc. 2015, 137, 5066–5073

tional to the gradient of binding site density, $F(x_0, y_0) = Q\nabla\rho(x_0, y_0)$. Substituting this into eq 2 yields the following:

$$v(x_0, y_0) = \frac{Q}{k_B T} D(x_0, y_0)\nabla\rho(x_0, y_0) \quad (3)$$

where except for the proportionality factor Q, all values can be experimentally determined. To verify this model, we performed a fit of the model to the normalized experimental intensity traces and obtained the drift velocity profile (Figure 5c), which interestingly is comparable to the transport velocities of biomolecular motors such as kinesin.[37] The value of the proportionality factor, Q, obtained from the fitting is $20k_BT$, which is within the range expected for electrostatic and van der Waals interactions of the multicharged pyranine with the charged hydrogel matrix in aqueous environment. Figure 6, parts ai and bi, compare snapshots of experimental intensity traces with the modeled concentration traces during the collection of pyranine by the narrow and wide cationic-to-neutral (tertiary amine-to-pristine PAAm) gradients (see SI Figure S12 for detailed comparison). For both systems, the model captures the overall spatial distribution and relative concentration of the cargo molecules observed in experiments. A more quantitative validation for the agreement between experiment and model is obtained by comparing the collection efficiency of the systems,

$$\eta_S = \frac{\int_S I(x, y)\, dxdy}{\int_T I(x, y)\, dxdy} \quad (4)$$

where S is the gradient region in the center of the gel film, T is the area of the entire gel film, and I is the normalized intensity/concentration for the experimental/modeled system, respectively. Figure 6, parts aii and bii, shows the experimental (circles) and modeled efficiency (solid line) obtained for both systems depicted in parts ai and bi at different times. The model shows good agreement with the experimental results, indicating that it describes the directed concentration by both gradient systems. The collection process can be divided into three time regimes, indicated by changes in the slope of the collection efficiency curves at different times for both the narrow and wide cationic-to-neutral gradients (Figure 6, parts aii and bii). At very short times (regime 1), before molecules reach the gradient, the efficiency is near zero, as an insignificant number of molecules pass from the gradient-free region of the substrate to the outer boundary of the gradient region toward the center of the substrate. This regime is more obvious in the narrow gradient (Figure 6a). At intermediate times (regime 2), once a significant number of molecules reach the gradient, the slope increases rapidly. At longer times (regime 3) the slope decreases, as the only molecules left to be collected are those that initially diffused away from the gradient region. We note that the collection forms a depletion region at the edge of the gradient (visible in Figure 4, parts aiii and biii, Figure 6ai, and SI Figure S12) caused by molecules being swept into the center by the gradient faster than they are replaced by freely diffusing molecules from outside the gradient. The velocity profile (Figure 5c) obtained from the fit also exhibits good agreement with the one obtained from theoretical model, indicating that the model captures the dependence of velocity on binding site density, and that the assumptions taken are valid within the resolution obtained in the experimental setup.

CONCLUSIONS

Enthalpy gradient-directed molecular transport in chemically patterned hydrogel films has been experimentally demonstrated and modeled. By controlling the synthetic conditions, gradients of different strength, length, and shape can be fabricated. The directed transport, concentration, and separation of molecules were demonstrated. The model accurately captures the behavior of molecules in the gradient, opening the way for designing gradient gel systems for specific requirements. Such gradient-directed molecular transport achieved velocities comparable to those of biomolecular motors such as kinesin[37] and offers the possibility for autonomous molecular processing. We believe that appropriately designed enthalpy gradients will provide previously unavailable opportunities for advanced chemical sensors and devices capable of manipulating complex mixtures of chemicals.

ASSOCIATED CONTENT

Supporting Information

Detailed experimental procedures, additional results and discussions of gradient fabrication and characterization, as well as simulation of the directed molecular transport. This material is available free of charge via the Internet at http://pubs.acs.org.

AUTHOR INFORMATION

Corresponding Authors

*pbraun@illinois.edu
*hh2374@columbia.edu

Present Addresses

[‖]3 M Company, 3 M Center, St. Paul, MN 55144, United States.
[#]Department of Chemistry, University of Idaho, Moscow, ID 83844−2343, United States.

Author Contributions

◆These authors contributed equally.

Notes

The authors declare no competing financial interest.

ACKNOWLEDGMENTS

This work was supported by DTRA under award numbers HDTRA 1-12-1-0035 (C.Z., H.J.K., K.V.W., P.V.B.) and HDTRA1-12-1-0037 (A.S., H.H.). The authors thank Dianwen Zhang and Scott Robinson (Beckman Institute, Illinois), Glenn Fried and Mayandi Sivaguru (Institute for Genomic Biology, Illinois), and Rudiger Laufhutte (School of Chemical Sciences, Illinois) for technical advice and support. A.S. acknowledges a Fulbright scholarship (United States-Israel Educational Foundation) and a Raymond and Beverly Sackler fellowship, Columbia University, for support.

REFERENCES

(1) Marre, S.; Jensen, K. F. *Chem. Soc. Rev.* **2010**, *39*, 1183−1202.
(2) Theberge, A. B.; Courtois, F.; Schaerli, Y.; Fischlechner, M.; Abell, C.; Hollfelder, F.; Huck, W. T. S. *Angew. Chem., Int. Ed.* **2010**, *49*, 5846−5868.
(3) Jebrail, M. J.; Bartsch, M. S.; Patel, K. D. *Lab Chip* **2012**, *12*, 2452−2463.
(4) You, I.; Yun, N.; Lee, H. *ChemPhysChem* **2013**, *14*, 471−481.
(5) Kay, E. R.; Leigh, D. A.; Zerbetto, F. *Angew. Chem., Int. Ed.* **2007**, *46*, 72−191.
(6) Bath, J.; Turberfield, A. J. *Nat. Nanotechnol.* **2007**, *2*, 275−284.

DOI: 10.1021/jacs.5b00240
J. Am. Chem. Soc. 2015, 137, 5066−5073

(7) Hess, H. *Annu. Rev. Biomed. Eng.* **2011**, *13*, 429−450.
(8) Brandley, B. K.; Schnaar, R. L. *Dev. Biol.* **1989**, *135*, 74−86.
(9) Chaudhury, M. K.; Whitesides, G. M. *Science* **1992**, *256*, 1539−1541.
(10) Ichimura, K.; Oh, S.-K.; Nakagawa, M. *Science* **2000**, *288*, 1624−1626.
(11) Daniel, S.; Chaudhury, M. K.; Chen, J. C. *Science* **2001**, *291*, 633−636.
(12) Smith, J. T.; Tomfohr, J. K.; Wells, M. C.; Beebe, T. P.; Kepler, T. B.; Reichert, W. M. *Langmuir* **2004**, *20*, 8279−8286.
(13) Keenan, T. M.; Folch, A. *Lab Chip* **2008**, *8*, 34−57.
(14) Ishii, D.; Shimomura, M. *Chem. Mater.* **2013**, *25*, 509−513.
(15) Walder, R.; Honciuc, A.; Schwartz, D. K. *Langmuir* **2009**, *26*, 1501−1503.
(16) Chang, T.; Rozkiewicz, D. I.; Ravoo, B. J.; Meijer, E. W.; Reinhoudt, D. N. *Nano Lett.* **2007**, *7*, 978−980.
(17) Burgos, P.; Zhang, Z.; Golestanian, R.; Leggett, G. J.; Geoghegan, M. *ACS Nano* **2009**, *3*, 3235−3243.
(18) Perl, A.; Gomez-Casado, A.; Thompson, D.; Dam, H. H.; Jonkheijm, P.; Reinhoudt, D. N.; Huskens, J. *Nat. Chem.* **2011**, *3*, 317−322.
(19) Klepárník, K.; Boček, P. *BioEssays* **2010**, *32*, 218−226.
(20) Rabilloud, T.; Chevallet, M.; Luche, S.; Lelong, C. *J. Proteomics* **2010**, *73*, 2064−2077.
(21) Sheehan, P. E.; Whitman, L. J. *Nano Lett.* **2005**, *5*, 803−807.
(22) Katira, P.; Hess, H. *Nano Lett.* **2010**, *10*, 567−572.
(23) Fang, J.; Park, S.; Schlag, L.; Stauden, T.; Pezoldt, J.; Jacobs, H. O. *Adv. Funct. Mater.* **2014**, *24*, 3706−3714.
(24) Bae, Y. H.; Park, K. *J. Controlled Release* **2011**, *153*, 198−205.
(25) Brannon-Peppas, L.; Blanchette, J. O. *Adv. Drug Delivery Rev.* **2004**, *56*, 1649−1659.
(26) Amsden, B. *Macromolecules* **1998**, *31*, 8382−8395.
(27) Park, S. H.; Kim, K.; Kim, M. S. *J. Mol. Struct.* **1993**, *301*, 57−64.
(28) Lee, E.; Yi, S. S.; Kim, M. S.; Kim, K. *J. Mol. Struct.* **1993**, *298*, 47−54.
(29) Lueck, H. B.; Swinney, T. C.; Hudson, B. S.; Friedrich, D. M. *Chem. Phys. Lett.* **1996**, *258*, 80−86.
(30) Gupta, M. K.; Bansil, R. *J. Polym. Sci., Part B: Polym. Phys.* **1981**, *19*, 353−360.
(31) Shinohara, H.; Yamakita, Y.; Ohno, K. *J. Mol. Struct.* **1998**, *442*, 221−234.
(32) Neugebauer, J.; Baerends, E. J.; Efremov, E. V.; Ariese, F.; Gooijer, C. *J. Phys. Chem. A* **2005**, *109*, 2100−2106.
(33) Nishiyabu, R.; Kubo, Y.; James, T. D.; Fossey, J. S. *Chem. Commun.* **2011**, *47*, 1106−1123.
(34) Fatin-Rouge, N.; Milon, A.; Buffle, J.; Goulet, R. R.; Tessier, A. *J. Phys. Chem. B* **2003**, *107*, 12126−12137.
(35) Nilsson, L. G.; Nordenskiold, L.; Stilbs, P.; Braunlin, W. H. *J. Phys. Chem.* **1985**, *89*, 3385−3391.
(36) Johansson, L.; Skantze, U.; Lofroth, J. E. *J. Phys. Chem.* **1993**, *97*, 9817−9824.
(37) Agarwal, A.; Katira, P.; Hess, H. *Nano Lett.* **2009**, *9*, 1170−1175.

DOI: 10.1021/jacs.5b00240
J. Am. Chem. Soc. 2015, 137, 5066−5073